Partial Volume Effect correction in PET using regularized iterative deconvolution with variance control based on local topology

A. S. Kirov[1], J. Z. Piao[2], C. R. Schmidtlein[1]

[1]Memorial Sloan-Kettering Cancer Center, New York, NY 11021, USA
[2]The Cleveland Clinic, Cleveland, OH 44195

E-mail: kirova@mskcc.org

Abstract. Correcting PET images for the partial volume effect (PVE) due to the limited resolution of PET has been a long standing challenge. Various approaches including incorporation of the system response function in the reconstruction have been previously tested. We present a post-reconstruction PVE correction based on iterative deconvolution using a 3D Maximum Likelihood Expectation-Maximization (MLEM) algorithm. To achieve convergence we used a One Step Late (OSL) regularization procedure based on the assumption of local monotonic behavior of the PET signal following Alenius *et al*. This technique was further modified to selectively control variance depending on the local topology of the PET image. No prior "anatomic" information is needed in this approach. An estimate of the noise properties of the image is used instead. The procedure was tested for symmetric and isotropic deconvolution functions with gaussian shape and full width at half-maximum (FWHM) ranging from 6.31 mm to infinity. The method was applied to simulated and experimental scans of the NEMA NU 2 image quality phantom with the GE Discovery LS PET/CT scanner. The phantom contained uniform activity spheres with diameters ranging from 1 cm to 3.7 cm within uniform background. Optimal sphere activity to variance ratio was obtained when the deconvolution function was replaced by a step function few voxels wide. In this case the deconvolution method converged in ~ 3 to 5 iterations for most points on both the simulated and experimental images. For the 1 cm diameter sphere, the contrast recovery improved from 12 % to 36 % in the simulated and from 21% to 55 % in the experimental data. Recovery coefficients between 80% and 120% were obtained for all larger spheres, except for the 13 mm diameter sphere in the simulated scan (68%). No increase in variance was observed except for few voxels neighboring strong activity gradients and inside the largest spheres. Testing the method for patient images increased the visibility of small lesions in non-uniform background and preserved overall image quality. Regularized iterative deconvolution with variance control based on the local properties of the PET image and on estimated image noise is a promising approach for partial volume effect corrections in PET.

1. Introduction

Finite scanner resolution prevents quantification for objects with size comparable and smaller than about 2-3 times the Full Width at Half-Maximum (FWHM) of the scanner's point spread function (PSF). This loss of quantitative accuracy for hot and cold spot contrast recovery for imaged objects is an effect known as partial volume effect (PVE) (Hoffman *et al.*, 1979; Hoffman *et al.*, 1982; Kessler *et al.*, 1984). The finite PET scanner resolution is due to the positron range prior to annihilation, positronium residual momentum at annihilation, which causes annihilation photon non-colinearity, finite crystal size, inter-crystal scatter, depth of penetration uncertainty, detector discretization, and artifacts introduced by the re-binning and reconstruction algorithms (Phelps *et al.*, 1975; Levin and Hoffman, 1999; Sanchez-Crespo *et al.*, 2004; Tomic *et al.*, 2005 ; Alessio *et al.*, 2006).

Various approaches for correcting the PVE have been previously tested. One possible classification of these methods was recently published(Soret *et al.*, 2007). It divides them into two large groups depending on whether the correction was applied at regional level targeting improved quantification for a selected region or on a voxel level, targeting resolution correction of entire images. On the other hand the methods, which specifically use the PET system response, can also be divided into two broad categories.

The first category includes methods, which account, and thereby correct, for the point spread function during the reconstruction. Earlier works in this direction include combining a Fourier transform of the positron range distribution function with the Fourier transform of the reconstruction filter in filtered back projection (FBP) reconstruction (Haber *et al.*, 1990). Penalized maximum likelihood algorithm has been used to correct the projections from the sinogram for a modeled detector response before filtering in filtered back projection algorithm(Liang, 1994). PSF deconvolution of rebinned 3D data prior to 2D reconstructions have also been performed.(Alessio *et al.*, 2006) One of the recent and most comprehensive methods incorporates an accurate model of the overall spatially variant PET system response in the projection matrix of a statistical reconstruction algorithm (Alessio and Kinahan, 2006). In an even more recent paper, deconvolution was performed prior to each subsequent iteration during Ordered Sub-sets Expectation Maximization (OSEM) reconstruction (Rizzo *et al.*, 2007).

The second category includes methods, which apply a resolution correction to the PET images post reconstruction. Most of these methods calculate in one way or another the PET signal spill-over from one structure to another and then attempt to correct for it (Rousset *et al.*, 1998). All of these methods either use prior anatomic information to define the volumes of elevated activity and to control variance within the rest of the image or do not address the increase in variance (Teo *et al.*, 2007). However, the assumption that the regions with elevated PET tracer concentration (TC) conform to the anatomical structures is not correct for oncologic studies, where the metabolically active tumor often may not fill an entire organ as defined by Computer Tomography (CT) or Magnetic Resonance Imaging (MRI) or may protrude in the neighboring tissues.

Therefore such methods are subject to some degree to at least one of the following two disadvantages, which decrease their potential for clinical use: i) unacceptable increase of variance in the image; ii) bias due to image registration or biology/metabolism based mismatch between TC and the anatomical information from CT or MRI.

In this paper we present a PVE correction method that is based upon post reconstruction iterative deconvolution. We tested deconvolution functions with shapes different from the scanner's point spread function. In order to avoid an increase in variance, we applied and modified the One Step Late (OSL) regularization procedure (Alenius and Ruotsalainen, 1997a). It was modified to impose variable penalty based on the local topology of the PET signal, avoiding in this way any dependence upon tracer uptake conformity with anatomical information. The method was tested on simulated and real PET phantom scans.

While this paper was in review, a conference report (Boussion *et al.*, 2007), describing a PVE correction method operating at the voxel level, which also does not depend on anatomical information and is based on a different, fully automatic, wavelet based de-noising approach appeared.

2. Methods and Materials

2.a. Deconvolution algorithm

The iterative three-dimensional deconvolution program is obtained by replacing the projection kernel in a MLEM algorithm for SPECT (Wallis and Miller, 1993) by a user defined point spread function (Kirov *et al.*, 2005). The tracer concentration (TC) estimated from the PET scan, C_a, is a result of a 3D convolution:

$$C_a(\vec{u}) = P(\vec{u} \mid \vec{r}) \otimes C_b(\vec{r}), \tag{1}$$

where $\vec{r}$ and $\vec{u}$ are three-dimensional coordinates in the measurement space, $P(\vec{u} \mid \vec{r})$ is the point spread function (PSF) value for the displacement vector, $\vec{r} - \vec{u}$, and $C_b(\vec{r})$ is the true TC distribution to be retrieved. The non-negativity of the TC and the point spread function allows us to use Csiszar's I-divergence (Csiszar I, 1991) as a discrepancy measure within MLEM. The estimate of the true TC, $\hat{C}_b(\vec{r})$, after k+1 iterations is then given by:

$$\hat{C}_b^{\,k+1}(\vec{r}) = \hat{C}_b^{\,k}(\vec{r}) \frac{1}{\sum_{\vec{u} \in A(\vec{r}, R_{PSF})} P(\vec{u} \mid \vec{r})} \sum_{\vec{u} \in A(\vec{r}, R_{PSF})} \left[\frac{C_a(\vec{u})}{\sum_{\vec{r}' \in B(\vec{u}, R_{PSF})} P(\vec{u} \mid \vec{r}') \hat{C}_b^{\,k}(\vec{r}')} \right] P(\vec{u} \mid \vec{r}), \tag{2}$$

where $\hat{C}_b^{\,k}(\vec{r}')$ is the TC distribution estimate after k iterations. By comparing the terms in (2) to these in (1), one can see that the next estimate of the TC in each voxel is obtained by multiplying the current estimate by the sum of the inaccuracy ratios for each of the neighboring voxels from the current estimate weighted by the corresponding PSF values $P(\vec{u} \mid \vec{r})$. A measure, $\varepsilon(\vec{u})$, of the inaccuracy of the kth estimate at voxel $\vec{u}$ can be expressed using the term in (2) representing this ratio:

$$\varepsilon(\vec{u}) = \left[\frac{C_a(\vec{u})}{\sum_{\vec{r}' \in B(\vec{u}, R_{PSF})} P(\vec{u} \mid \vec{r}') \hat{C}_b^{\,k}(\vec{r}')} \right] - 1 \tag{2.a}$$

The effect of the PSF to each voxel $\vec{u}$ is limited to a cubic region with side $2*R_{PSF}+1$ voxels centered at $\vec{u}$, where R_{PSF} is a user defined parameter.

Since the direct implementation of (2) results in limited contrast recovery accompanied with strong variance increase(Snyder *et al.*, 1987), in this paper we depart from the common assumption that the PSF, $P(\vec{u}\,|\,\vec{r})$, needs to match the scanner point spread function, which is often approximated by a Gaussian type function. In fact, we suggest using a function that is more slowly varying than the scanner PSF. From here forward we will refer to it as the deconvolution function (DF). We expect that using such slowly varying DF will:

1) Limit variance increase throughout the image by calculating the inaccuracy ratios, $1+\varepsilon(\vec{u})$ in (2) with respect to activity closer to the mean activity of the region $B(\vec{u}, R_{PSF})$ around the voxel, rather than with respect to the activity estimate for voxel $\vec{u}$, which it represents when the scanner PSF is used.
2) Reduce variance in the uniform activity regions by more equally weighted averaging of the inaccuracy ratios $1+\varepsilon(\vec{u})$ of the previous (k^{th}) activity estimate within the region around each voxel. (A Gaussian shaped PSF will give larger weight to the inaccuracies closer to the center of the Gaussian, which may be noisier.)
3) Enhance the deconvolution for the regions that have stronger activity variation (i.e. tumor edges), where the inaccuracy measure $1+\varepsilon(\vec{u})$ is expected to have both larger values and variation.

This modification of the deconvolution procedure has a strong theoretical background. In general any deconvolution of noisy data is an attempt to solve an ill-posed mathematical problem if the solution is being searched among all possible functions. In the case of PET, that would be all mathematically possible activity distributions (Fedorenko, 1994). Real activity distributions are expected to be smoother than PET images with limited statistics, which are noisy. Therefore, the correctness can be improved if the solution is limited to a narrower space of smoother functions. This is what, we expect, the substitution of the scanner PSF with a more slowly varying function will accomplish: using a more uniform, i.e. broader width, PSF, will effectively impose stronger smoothness on the solution and thereby will improve the correctness of the problem. In this way it is introducing additional regularization to the One Step Late regularization described in § 2.b below.

To show this we varied the point spread function's FWHM. We tested Gaussian shape DFs with FWHM of 6.31 mm, 18.93 mm (= 6.31x3), 31.55 mm (= 6.31x5), and an infinite value (i.e. a step function).

To enhance convergence a Median Root Prior (MRP) filter (Alenius and Ruotsalainen, 1997b) is implemented (Piao and Kirov, 2001, Kirov *et al.*, 2005). using a One Step Late (OSL) MRP algorithm:

$$\hat{C}_b^{\,k+1}(\vec{r}) = \frac{\hat{C}_b^{\,k+1,dec}(\vec{r})}{1+\beta\,\dfrac{\hat{C}_b^{\,k}(\vec{r}) - M_R}{M_R}}. \qquad (3)$$

Here, $\hat{C}_b^{(k+1),dec}(\vec{r})$ is the $(k+1)^{th}$ estimate of the emission density in voxel at position $\vec{r}$ after the PSF deconvolution (1) but before MRP regularization, $\hat{C}_b^{(k)}(\vec{r})$ and

$\hat{C}_b^{(k+1)}(\vec{r})$, are the kth and (k+1)th estimates of the emission density at position $\vec{r}$ after the MRP penalization, $M_R = Med(\hat{C}_b^k, \vec{r}, R)$ is the median voxel value in a small neighborhood with radius *R*, around the voxel at $\vec{r}$, and β is the weight of the prior.

2.b. Topology adaptive regularization

The regularization parameters in (3) are the weight β and the radius of the neighborhood *R* for calculating M_R. In order to restrict the variance increase in the images we varied the weight β, so that stronger regularization is applied to background parts of the image. Regions close to the image edges were also assigned stronger regularization (β_1) to suppress the known edge artifacts of the ML algorithm. Regions with activity variations larger than the background noise, which could reveal potential lesions, were assigned weaker regularization (β_2).

To do this we select two more neighborhoods around each point in which to check the minimum activity and the variation of activity against fractions (k_1 and k_2) of the background value. These two neighborhoods would generally have different radii (R_1 and R_2), smaller than R, in order to preserve the gradients in these regions of the image.

For a neighborhood with radius R_1 around each voxel, we find the minimum activity voxel, $P_{min,R1}$, and for a neighborhood with radius R_2 we find the minimum, $P_{min,R2}$, and the maximum, $P_{max,R2}$, voxel values. Let M_{bkg} be a rough estimate of the entire image's background level (note that M_{bkg} is not the same as M_R used above and can be visually determined by observing activity profiles through the images). Then the PET image data set can be effectively divided into three parts: regions of interest in which the activity undergoes a change above a certain threshold (regularized with weight β_2), background regions (regularized with β_0), and regions around the image edges (regularized with β_1) following these conditions:

$$\beta = \begin{cases} \beta_0 & \textit{elsewhere} \\ \beta_1 \quad \text{for} & P_{\min,R_1} < k_1 \cdot M_{bkg} \\ \beta_2 & \left| P_{\max,R_2} - P_{\min,R_2} \right| > k_2 \cdot M_{bkg} \end{cases} , \qquad (4)$$

where R_1, R_2, , k_1, k_2 and M_{bkg} as well as β_0, β_1 and β_2 are parameters set by the user. While these parameters seem many, they do represent a clear example of how one can intuitively adapt the strength of the regularization to the image topology. In fact these parameters represent an efficient approach to assign an appropriate value for the regularization weight, β, in different parts of the image. As shown in the results section (3.1.b) they turned to have stable values for the tested images.

The algorithm proceeds as follows. A weight value $\beta = \beta_0$ is initially assigned for the entire data set for each PET scan. This value is relatively high (~ 0.9) and is set to control variance in the background portions of the images, where increase of variance due to the deconvolution needs to be suppressed most.

Next, a check corresponding to the second line of (4) may change β if it is close to regions with PET signal significantly lower than the average image background (k_1 ~ 0.3), i.e. around air cavities or outside the patient. This check imposes an even higher regularization weight (β ~ 1), which is necessary to penalize the so called "edge artifacts"(Snyder *et al.*, 1987) of the MLEM algorithm. This artifiact usually manifests as elevated activity at the surface of the patient's skin.

Finally, a check corresponding to the third line of (4) may reduce β to a lower value, β_2, for regions in which the PET signal fluctuations exceed an empirically determined fraction of the background signal, M_{bkg}. These regions would correspond to noticeable activity changes for which the weaker penalty allows stronger deconvolution.

The user selects what fraction, k_2, of the background activity level would be considered noise. For activity changes larger than $k_2 \cdot M_{bkg}$, the regularization is relaxed since they would be considered significant. For both the simulated and experimental phantom scans, the magnitude of these "noticeable" activity variations was determined to be close to the magnitude of the background signal ($k_2 \sim 0.9$). In the clinic this threshold value will be probably determined by a radiologist.

2.c. Scanner and phantoms

The deconvolution program was applied to simulated and real images of the NEMA NU 2 image quality phantom obtained using the GE Discovery LS PET/CT (DLS) scanner.

The simulated data was obtained with the GATE (Geant4 Application for Tomographic Emission) Monte Carlo (MC) code for the case of higher (14.98 kBq/mL) activity concentration in the 10,13,17, and 22 mm diameter spheres, no activity in the 28 and 37 mm diameter spheres, and lower (3.98 kBq/mL) activity concentration in the rest of the phantom. We used a previously validated GATE MC model of this scanner in 3D mode (Schmidtlein *et al.*, 2006; Schmidtlein *et al.*, 2005). The data was reconstructed with MLEM using the Software for Tomographic Image Reconstruction (STIR). The images contained 256 x 256 voxels with 2.14844 mm size in the x and y directions and 4.25 mm in the z direction.

The experimental data was obtained using 2D High Resolution mode using our clinical settings on a GE Discovery LS PET/CT scanner. In the experiment, all six spheres were filled with an activity concentration of 21.98 kBq/mL and background activity was 5.5 kBq/mL. The data was collected using a 15 min acquisition and reconstructed with the MLEM algorithm of the scanner. The images contained 128 x128 voxels with 4.6875 mm size in the x and y directions and 3.27 mm in the z direction.

The mean contrast recovery coefficients (RC) were calculated as outlined in the NEMA NU2 protocol(NEMA, 2001), using circular regions inside the spheres in the central slice and 60 circular regions for the background around them.

The method was also tested for a patient PET scan obtained in our clinic on the Discovery LS PET/CT scanner using ^{18}F-fluoro-deoxyglucose (FDG) in 2D mode. The images contained 128 x128 voxels with 3.90625 mm size in the x and y directions and 4.25 mm in the z direction.

2.d. Deconvolution and regularization parameters

For the deconvolution weighting function we tested a symmetric 3D Gaussian with Full Width at Half Maximum (FWHM) varying from 6.31 mm (the approximate mean PSF of the scanner) to infinity. The radius of this function was varied from 2 to 3 voxels for the experimental scans and from 3 to 6 voxels for the simulated data to reflect the difference in voxel size between the two images.

Alenius (Alenius, 1999) suggested that the radius R of the monotonicity neighborhoods should be selected to approximate the width of the smallest detail to be preserved. We selected R_1 and R_2 to approximate the width of the high gradient regions at the edges of the image and of the spheres.

The regularization weights, β_0, β_1 and β_2, were optimized to satisfy the following criteria: i) to reach convergence ; ii) to obtain recovery coefficients closest to unity for all spheres; iii) to control increase of variance in the background regions and the phantom edges and thereby to obtain smoother images with better visible lesions and less artifacts. For monotonicity neighborhoods 3 voxels wide $\beta \sim 0.3$ was previously suggested (Alenius, 1999) and we tested similar values for the areas of interest in the image containing elevated activity. Values for β_0 and β_1 closer to 1.0 (Alenius and Ruotsalainen, 1997b), were experimented for the background and edge regions to suppress variance. Alenius *et al* (Alenius and Ruotsalainen, 1997b) have shown convergence for this range of values.

The background activity parameter M_{bkg} was obtained by a visual estimate of an activity profile observation (Fig.2) to approximate the average PET image background level. It is specific for each image and was selected to be 3800 and 5000, which approximate the background activity levels in Bq/mL for the simulated and the experimental images respectively.

The fractions k_1 and k_2 of the background TC, M_{bkg} , were selected by observing the image to give TC threshold values of less than a fraction (~1/3) of M_{bkg}, for k_1, and exceeding the maximum TC variance (~35%) in the background part of the image, for k_2. The optimal parameters found are given in Table 1.

The PVE correction (we did not need to test more than 14 iterations) takes about 15-20 min. for the simulated 256x 256 pixel images and less than 5 min. for the experimental 128 x 128 mm images on a 3.2 GHz CPU. The computation time depends upon the deconvolution and regularization parameters used.

3. Results

PET images and activity profiles before and after applying the PVE correction are presented in Figures 1, 2, 4 and 6. The effects of the FWHM of the deconvolution function on the recovery of peak activity and on the signal to background fluctuations are presented in Fig. 3. The effect of the PVE correction on the recovery coefficients calculated following the NEMA NU 2 protocol is presented in Fig.5.

3.1. Parametric study

3.1.a. Deconvolution function

Without regularization (equation 3) no convergence of the iterative procedure (equation 2) is observed for any of the different deconvolution functions (DF) used. With regularization and using a gaussian shaped DF approximating the experimental PSF of the scanner (FWHM = 6.31 mm) resulted in insufficient recovery of the activity of the two smallest spheres accompanied with strong increase of variance, which reached the intensity of the smallest sphere at ~15 iterations. Increasing the

width of the DF enhanced the contrast recovery (Figures 2b and 3.). To investigate this we calculated the (Peak Activity in Sphere)/(Peak Activity in Background Fluctuations) ratios along the profile shown in Fig.2.b. In Figure 3 is plotted this ratio divided by the true signal over background ratio of 3.57 (= 14.2 kBq/mL / 3.98 kBq/mL).

The cut-off radius of the DF was also found to affect the strength of the deconvolution – larger radius leads to stronger deconvolution for both sets of data. Using radii of 4, 5, and 6 voxels for the simulated scan and radii of 2 and 3 voxels for the experimental scan (i.e. cubes with sides 5 and 7 voxels) resulted in similar quality images. Images with optimal contrast recovery and minimum image distortions with identical regularization parameters were observed when radii of 4 and 3 voxels were used for the two data sets respectively.

3.1.b. Regularization parameters

Imposing regularization on the deconvolution process enforced convergence within 3 to 5 iterations for both the simulated and the experimental data and brought the maximum activity in the spheres and the peak sphere to background ratios closer to those of the true values (Fig. 3). Additional iterations (up to 14) were found to have negligible effect on the result as shown in Figure 4. A set of regularization parameters found to work optimally for both data sets is shown in Table 1.

Table 1. Selected deconvolution and regularization parameters used for the simulated (top row) and experimental scans (bottom row).

Deconvolution function		Regularization parameters							
		Image		Edges			Peaks		
FWHM	R_{DF}	R	β	k_1	R_1	$\beta 1$	k_2	R_2	β_2
infinite	4	4	0.9	0.3	3	1.1	0.9	2	0.35
infinite	3	4	0.9	0.3	3	1.1	0.9	2	0.35

Applying an MRP penalty of $\beta = 0.9$ to the entire image limits the variance increase caused by deconvolution in the parts of the images with small activity changes. Such strong regularization was imposed on all voxels, which do not exceed M_{bkg} by more than 90% (k_2 = 0.9). The 90 % value was chosen to include all background regions with noise related fluctuations up to that threshold. Above that, a much weaker MRP regularization penalty of β_2 = 0.35 allows stronger, but yet controlled deconvolution in the peak activity regions close to the spheres. Selecting a layer of 3 voxels around the edges (R_1 = 3) of the phantom with even stronger regularization ($\sim\beta_1$=1.1) allows to control the MLEM edge artifacts(Snyder *et al.*, 1987).

As is illustrated in Figures 1, 2a, and 4, applying such topology dependent regularization allows reduction of the variance in background regions and PVE correction improvement in high gradient regions.

3.2. Recovery of activity profiles and mean contrast

The recovery of the activity profiles is illustrated in Figures 2 and 4.a and 4.b for the 10, 13, 22 and 28 mm spheres for the simulated scan and in Figure 4.c for the 10 and 37 mm spheres of the experimental scan.

The profiles of the spheres after the PVE correction are in general closer to the true activity profiles with the following exceptions: i) The central profile across some of the spheres may overestimate the true activity (Fig. 4.b); ii) Non-uniform uptake inside the larger spheres is amplified by the deconvolution (Fig. 4.c). Both of these artifacts are natural consequences of the deconvolution and if the regularization parameters are not carefully chosen this may lead to a substantial loss of mean contrast recovery accuracy.

In the background regions, due to the stronger regularization imposed in this portion of the image, the activity profile differs very little from the activity profiles prior to the PVE correction. An exception is presented by few voxels around the spheres and inside the largest spheres, in which a moderate increase in the variance is observed. Also a small increase of the edge artifacts occurs at the periphery of the phantom (Fig. 4.c). However, these are controlled by the regularization weight, β_1, and are difficult to see in the images (Fig. 1).

For the spheres with diameters between 10 and 22 mm a significant improvement of the RC is seen (Fig. 5). For these spheres the RC improves from pre-correction values of 13% to 60% before to 36% to 92% after PVE correction for the simulated data and from 21% to 71% before to 54% to 118% after the correction for the experimental scan. In both cases, the PVE correction presented in this paper reduces the bias in the RC to less than 20% for all spheres except for the 10 mm diameter sphere in the experiment and the 10 and 13 mm diameter spheres in the simulated data. For the largest spheres with diameter of 28 and 37 mm there is no improvement of the mean RC. This is independent from whether they are hot (experiment) or cold (simulation).

3.3. Test on a patient PET scan

Although the goal of this paper is to show proof of concept for the presented PVE correction method using phantom data, we present also a result for a FDG patient PET scan obtained in our clinic on the Discovery LS PET/CT scanner in 2D mode (Fig.6). The same parameters as for the phantom case were used except for the background activity, M_{bkg}, which was set to roughly approximate the middle of the background signal, 4000 Bq, and the coefficient k_2, for which a value of 3 was selected due to the stronger background variation and stronger uptake in the potential lesions. At 4 iterations the algorithm has converged. The corrected image shows enhanced uptake in certain parts of the image. Some of them could be potential lesions. Variance is not increased in the rest of the image.

Performing the correction with different values for these two parameters, k_2=4 for M_{bkg}=4000 Bq, limits the uptake enhancement to the two mediastinal lesions and the chest wall only. Selecting the background to match the highest background in the vicinity of these lesions (M_{bkg} = 7000 Bq) and k_2=2 results in enhancement of only the more laterally positioned lesion and the chest wall.

4. Discussion

4.1. Main features of the method

There are two main features of the post-reconstruction PVE correction method described in this paper, which make it different from previously published methods:

i) We changed the shape of the deconvolution function. In addition to a PSF approximating that of the scanner, we tested significantly broader functions with FWHM ranging to infinity. The last one, a step function over a cubic region centered at the voxel being corrected provided the best results.

ii) We adapted the regularization procedure to the topology (activity levels and activity variance) of the images, rather to prior "anatomic" information about the sphere size and position.

We have shown (Figure 2.b and 3.), that the first feature (i) leads to improved activity and contrast recovery. This result can be explained in the following way. The factor $[1 + \varepsilon(\vec{u})]$ (2.a), updates the activity estimate in the iteration formula (2) relative to the mean activity for the neighborhood of a voxel, rather than relative to the activity weighted closer to that of voxel $\vec{u}$ which would be the case for a sharper DF. This dampens variance increase in the background. Also using a more uniform DF, $P(\vec{u} \mid \vec{r})$, which multiples $[1 + \varepsilon(\vec{u})]$ in (2) reduces variance in the uniform activity regions by more equally weighted averaging of the inaccuracies (2.a) of the previous activity estimate over the selected region. A more uniform DF would also enhance deconvolution for the regions with stronger activity change due to giving more weight to the expected larger inaccuracy in such regions.

The above result is a direct consequence of improving the correctness of the mathematical problem by introducing additional regularization within the iterative sequence(Fedorenko, 1994). While one can argue that replacing the scanner PSF with a step function results in the loss of inherent information about the scanner, it turns out that regularization of the problem is more critical. The specifics of the scanner enter in the PVE correction through the truncation width of the deconvolution function (DF) and through the regularization parameters, which are tailored to the type of PET images being corrected.

The second feature, topology adapted regularization, is important in oncology where PET tracer uptakes do not necessarily conform to that of the anatomical structures identified with CT or MRI. Tumors may occupy only part of an anatomic structure or may protrude in the tissues between such structures or into neighboring organs.

4.2. Comparison to other methods

For uniform activity spheres the presented method yields activity and contrast recovery accuracy similar to the methods that incorporate the position and direction dependent detection system response into the reconstruction (Alessio and Kinahan, 2006). However, while that and also other methods(Soret *et al.*, 2007) use anatomical information to govern the penalty term, the method presented here does not. Higher recovery coefficient accuracy is demonstrated in a method based on the "regional geometric transfer matrix" (Rousset *et al.*, 1998). This method also uses anatomical information, which in that case is based on high resolution MR images. Another post-reconstruction PVE correction method (Teo *et al.*, 2007) also produced higher recovery coefficient accuracy, but in this paper the problem of variance increase throughout the image was left for future studies.

In the Soret *et al.* classification, the PVE correction methods are divided in two groups, which both have disadvantages: a) correction methods applied at regional

level which improve local contrast recovery, but are not suitable for visual image analysis; and b) correction methods applied at voxel level, which rely on joint use of anatomic information. The method presented here has the potential to resolve these problems: it simultaneously improves local contrast recovery (quantification), provides improved images for visual analysis, and does not rely on anatomic information.

According to a recent conference report, such capabilities were shown also for a different approach (Boussion *et al.*, 2007). The main difference between the two methods is that in the method of Boussion *et al*, the noise suppression is wavelet based and fully automatic. In our method the user would need to select few regularization parameters based on the properties of the PET images. In that respect it could be used to selectively enhance the PVE correction for parts of the image with physician selected levels of activity concentrations and activity concentration variations.

4.3 PVE correction for realistic cases with non-uniform background

The topology adaptive regularization algorithm presented in the current paper allows selective enhancement of deconvolution in the areas of elevated activity and successfully controls variance increases within the rest of the image, without using any prior anatomic information from CT or MRI studies. This was demonstrated also for a patient PET scan containing strong TC non-uniformity and potential mediastinal lung lesions.

For the presented patient image only two parameters needed to be changed with respect to the phantom cases: the background activity M_{bkg} and the factor k_2 , which determines the variation threshold above which the TC would be considered to be above the noise fluctuations. As pointed in §3.3 the modification of these parameters allows limiting the PVE correction to medically significant parts of the image. Other regularization parameters, e.g. the regularization weight β_2, may also need to be changed for large tumors with non-uniform uptake in order to limit variance increase within such lesions. We consider it prudent to leave the selection of the threshold separating noise from significant activity changes to the physician.

We foresee two possible ways of using the described PVE correction method: 1) by user selection of the regularization parameters, which can limit the strength and the threshold for enhancing TC variations to medically relevant regions and limits; 2) by using fixed parameters, previously optimized to give highest quantification accuracy for PET scans with similar properties. The successful implementation of either of these approaches requires further investigation. For the first approach, a large data base of PET scans will need to be analyzed together with radiologists and radiation oncologists for different tumor sizes, tumor locations and uptake uniformity distributions. For the second approach, an extensive validation of the method using optimized parameters against experimental or numerical phantoms with non-uniform uptake in known lesions needs to be performed.

Special attention to validation will be needed also when the PVE correction is applied to large tumors with heterogeneous uptake or lesions with steep boundaries, since the method will increase the variance for such regions. This is seen in the increased dip in the profile of the large sphere in Fig.4.c and in the small edge artifacts around the spheres in Fig.1. No such artifacts are however expected for small lesions due to more gradual uptake increase (Fig. 6 b and c).

5. Conclusion

Introducing a deconvolution function with a step function shape and topology adaptive regularization in maximum-likelihood based iterative deconvolution lays the basis of a novel approach for controlling image variance. Applying this method to a phantom with uniform activity spheres improved quantification accuracy without increasing variance in the rest of the image. Testing the method for patient images increased the visibility of small lesions in non-uniform background, while in the same time preserving image quality.

Two ways for clinical implementations are possible: 1) by user selection of the regularization parameters, which can limit the strength and the threshold for enhancing activity variations to medically important regions; 2) by using fixed parameters, previously optimized to give highest quantification accuracy for PET scans with similar properties. Both implementations depend on further evaluation and validation with extensive image sets and realistic phantoms with known lesions.

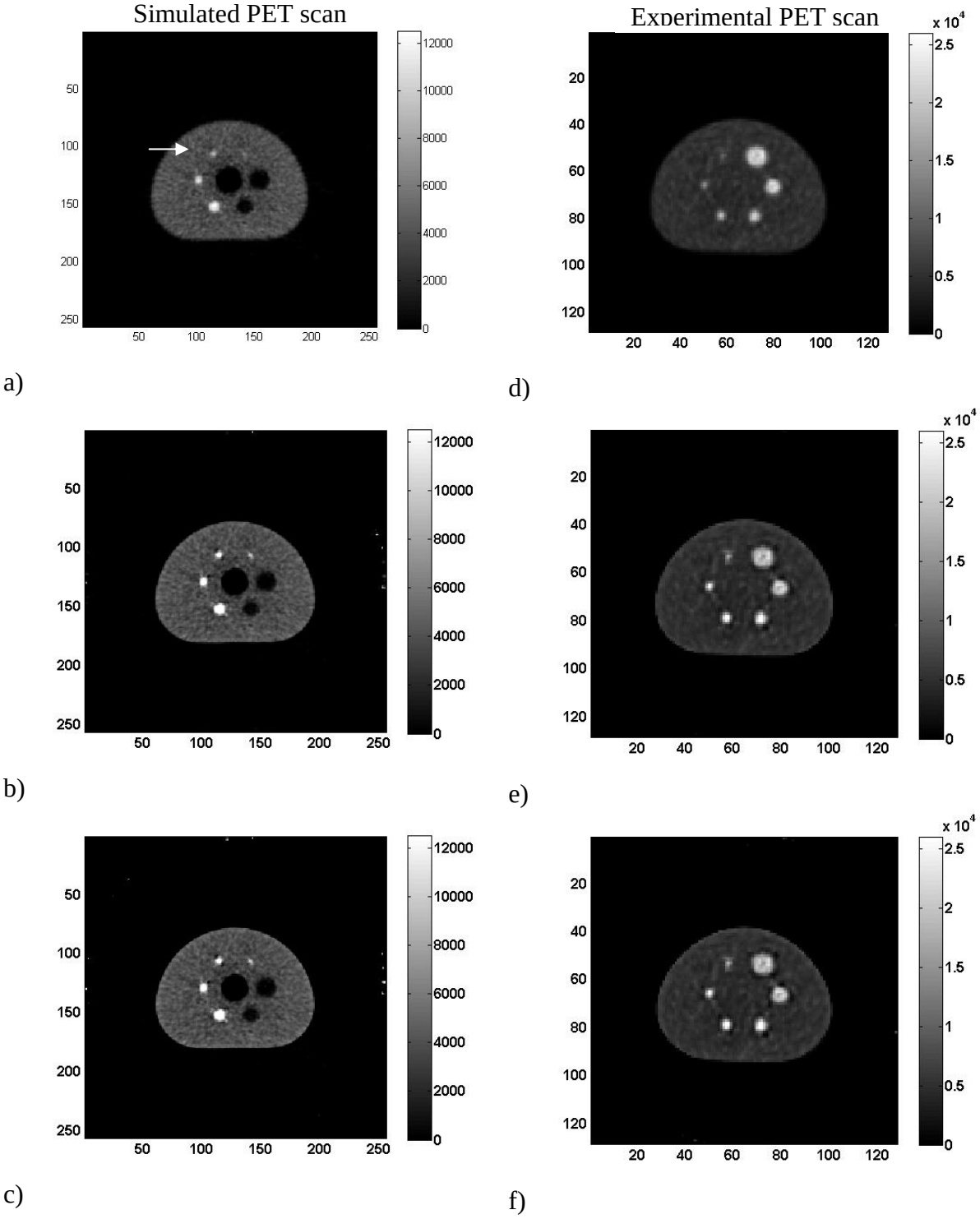

Fig. 1. PET images (in pixels and in Bq/pixel) of the NEMA NU 2 image quality phantom before (a,d) and after PSF deconvolution for simulated (left) and experimental scans (right) with 5 (b,e) and 15 iterations (c,f). The arrow in a) indicates the approximate position of the profiles drawn through each of the images and presented in Fig. 2.

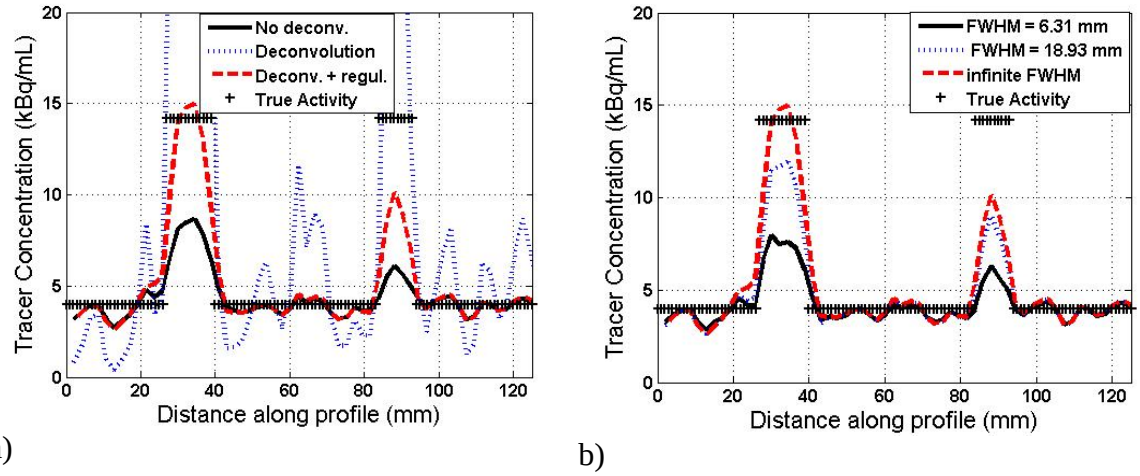

Fig. 2. a) Recovered activity concentration profiles across the smallest two spheres of the simulated PET scan (see arrow in Fig.1), before and after deconvolution, and after deconvolution with the described regularization, when a deconvolution function (DF) with infinite full width at half-maximum (FWHM) was used; b) Effect of the FWHM of the DF on the same profile when the same regularization parameters were used. 14 iterations were used in all cases. The crosses indicate the true activity levels.

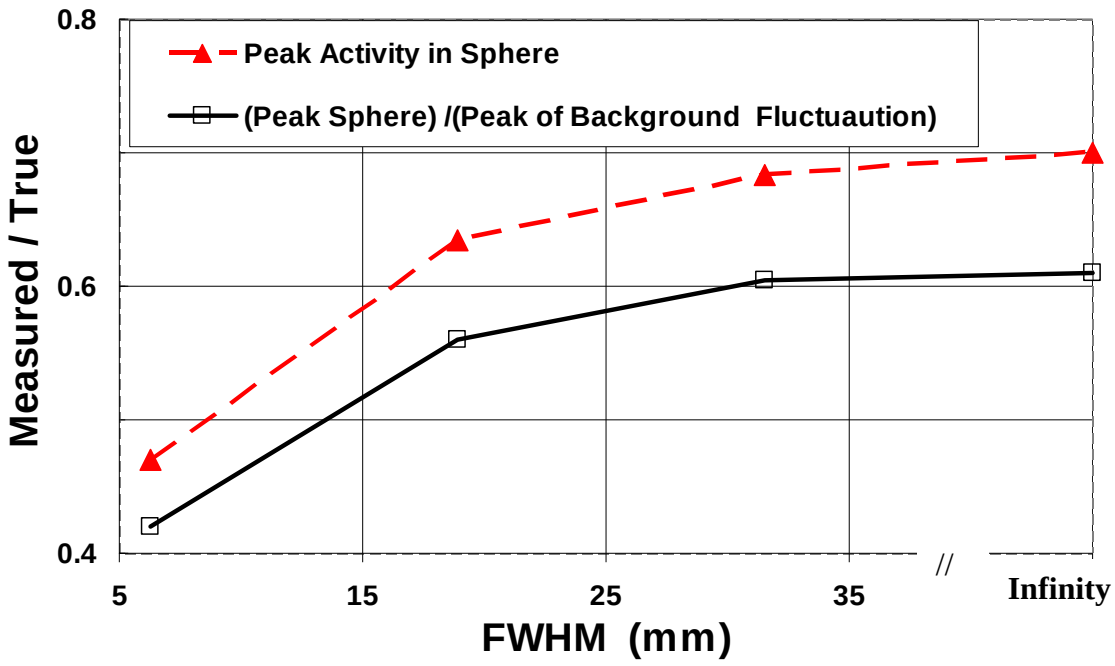

Fig.3. Measured over true ratios of the Peak Activity (triangles) and of the (Peak Sphere)/(Peak of Background Fluctuation) (squares) in the smallest, 10 mm diameter sphere, as a function of the FWHM of the deconvolution function. Some of the data points correspond to profiles displayed in Fig.2.b.

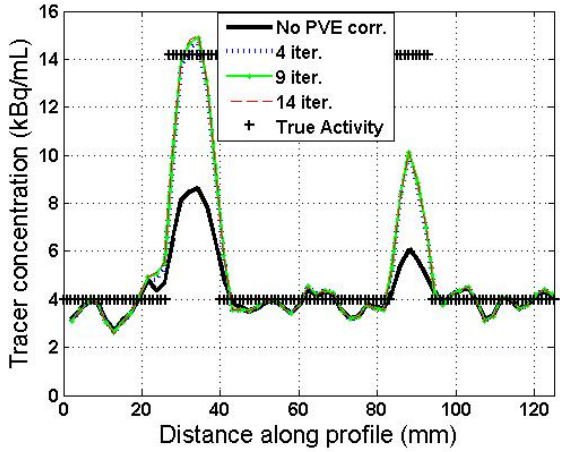

a)

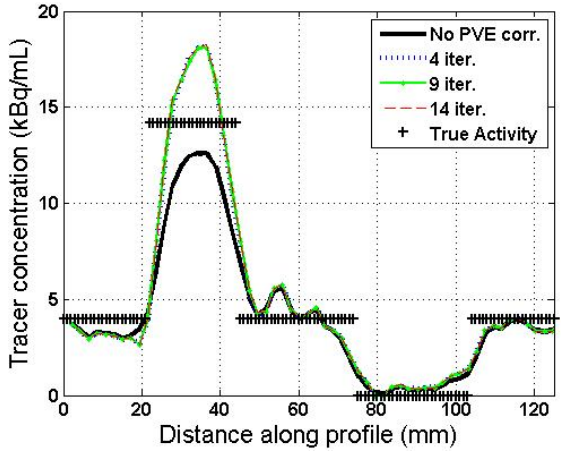

b)

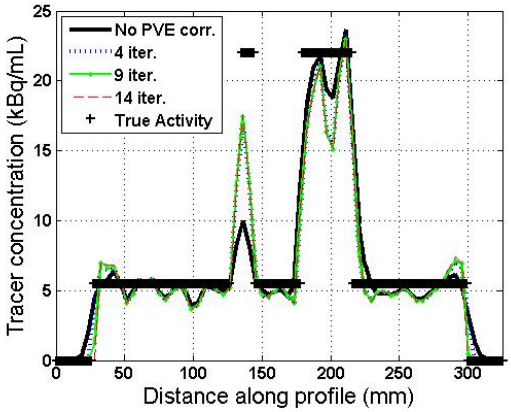

c)

Fig.4. Recovery of activity profiles passing through the center of the 13 and 10 mm (a) and the 22 and 28 mm (b) diameter spheres in a simulated scan, and of the 10 and 37 mm spheres in a measured scan (c) of the NEMA image quality phantom (Fig.1). The crosses indicate the true activity levels and their approximate location.

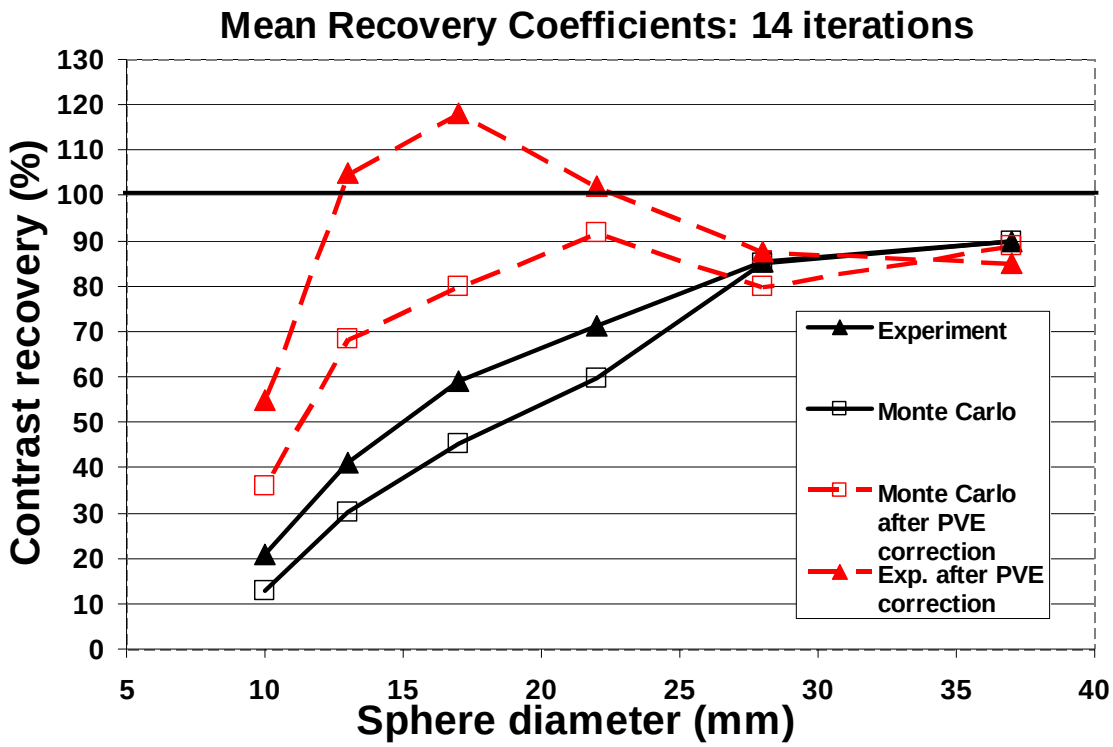

Fig.5. Mean contrast recovery before and after regularized deconvolution for simulated and experimental scans of the NEMA image quality phantom.

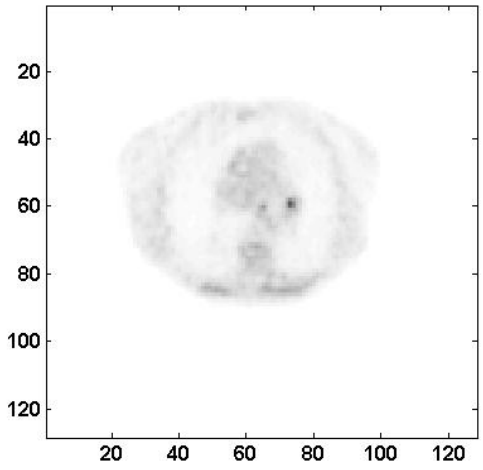

a)

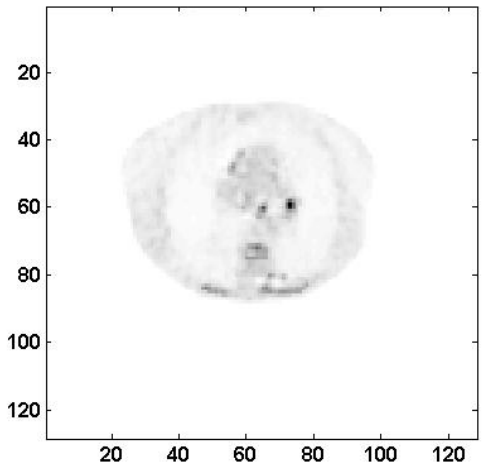

b)

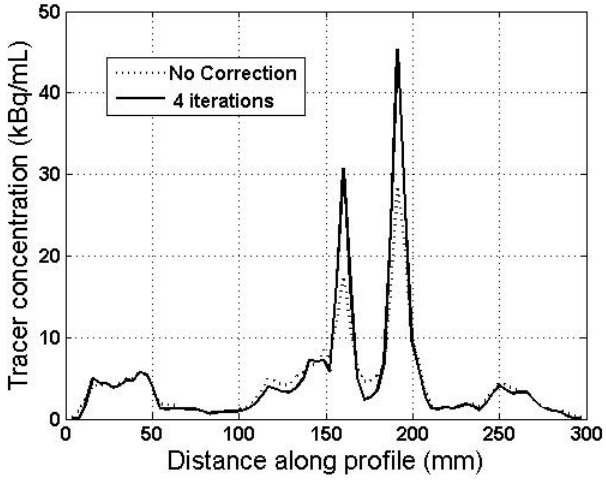

c)

Fig. 6. Transaxial PET slices of a lung cancer patient before (a) and after PVE correction (b) using the described method. Fixed inverse gray scale was used. Profiles through the two mediastinal potential lesions with and without the correction are shown in c).

References

Alenius S 1999 "On noise reduction in iterative image reconstruction algorithms for emission tomography: Median root prior", Ph.D. Thesis, Tampere University of Technology, Tampere, Finland.

Alenius S and Ruotsalainen U 1997a Bayesian image reconstruction for emission tomography based on median root prior *Eur. J. Nucl. Med.* **24** 258-65

Alenius S and Ruotsalainen U 1997b Bayesian image reconstruction for emission tomography based on median root prior *European journal of nuclear medicine* **24** 258-65

Alessio A, Sauer K and Kinahan P 2006 Analytical reconstruction of deconvolved Fourier rebinned PET sinograms *Physics in medicine and biology* **51** 77-93

Alessio A M and Kinahan P E 2006 Improved quantitation for PET/CT image reconstruction with system modeling and anatomical priors *Medical physics* **33** 4095-103

Boussion N, Hatt M, Reilhac A and Visvikis D 2007 "Fully Automated Partial Volume Correction in PET Based on a Wavelet Approach Without the Use of Anatomical Information", IEEE Nuclear Science Symposium and Medical Imaging Conference Record, Paper M12-5, Oct. 27 - Nov. 3 , 2007, Honolulu, HI, USA.

Csiszar I 1991 Why least squares and maximum entropy? An axiomatic approach to inference for linear inverse problems *Ann.Stat* **19** 2032-66

Fedorenko R P 1994 *Introduction to Computational Physics* (Moscow: MFTI (in Russian))

Haber S F, Derenzo S E and Uber D 1990 Application of Mathematical Removal of Positron Range Blurring in Positron Emission Tomography *IEEE Trans. Nucl. Sci.* **NS-37** 1293-9

Hoffman E J, Huang S C and Phelps M E 1979 Quantitation in positron emission computed tomography: 1. Effect of object size *Journal of computer assisted tomography* **3** 299-308

Hoffman E J, Huang S C, Plummer D and Phelps M E 1982 Quantitation in positron emission computed tomography: 6. effect of nonuniform resolution *Journal of computer assisted tomography* **6** 987-99

Kessler R M, Ellis J R, Jr. and Eden M 1984 Analysis of emission tomographic scan data: limitations imposed by resolution and background *Journal of computer assisted tomography* **8** 514-22

Kirov A S, Piao J Z, Mathur N K, Miller T R, Devic S, Trichter S, Zaider M, Soares C G and Losasso T 2005 The three-dimensional scintillation dosimetry method: test for a (106)Ru eye plaque applicator *Physics in medicine and biology* **50** 3063-81

Levin C S and Hoffman E J 1999 Calculation of positron range and its effect on the fundamental limit of positron emission tomography system spatial resolution *Physics in medicine and biology* **44** 781-99

Liang Z 1994 Detector response restoration in image reconstruction of high resolution positron emission tomography *IEEE transactions on medical imaging* **13** 314-21

NEMA 2001 Performance Measurements of Positron Emission Tomogrpahs, NEMA Standarts publication NU 2-2001. (Rosslyn, VA: National Electrical Manufacturers Association)

Phelps M E, Hoffman E J, Mullani N A and M.M. T-P 1975 Application of annihilation coincidence detection to transaxial reconstrution tomography *J Nuc. Med.* **16** 210-24

Piao Z and Kirov A S 2001 Effect of Median Root Prior (MRP) regularization on the accuracy and convergence of maximum likelihood expectation maximization algorithm applied to 3D scintillation dosimetry (abstract on the AAPM web-cite). In: *2001 Annual Meeting of the American Association of Physicists in Medicine,* (Salt Lake City, UT

Rizzo G, Castiglioni I, Russo G, Tana M G, Dell'Acqua F, Gilardi M C, Fazio F and Cerutti S 2007 Using deconvolution to improve PET spatial resolution in OSEM iterative reconstruction *Methods of information in medicine* **46** 231-5

Rousset O G, Ma Y and Evans A C 1998 Correction for partial volume effects in PET: principle and validation *J Nucl Med* **39** 904-11

Sanchez-Crespo A, Andreo P and Larsson S A 2004 Positron flight in human tissues and its influence on PET image spatial resolution *European journal of nuclear medicine and molecular imaging* **31** 44-51

Schmidtlein C R, Kirov A S, Bidaut L, Nehmeh S, Erdi Y, Ganin A, Stearns C W, McDaniel D L, Humm J and Amols H 2006 "Validation of GATE Monte Carlo simulations for the GE Advance/Discovery LS PET scanners" *Med. Phys.* **33** 198-208

Schmidtlein C R, Kirov A S, Bidaut L M, Nehmeh S A, Erdi Y E, Ganin A, Sterns C W, McDaniel D L, Hamacher K A, Humm J L and I A H 2005 Validation of GATE Monte Carlo Simulations of the Noise Equivalent Count Rate and Image Quality for the GE Discovery LS PET Scanner, Proc. of the AAPM 47th Annual Meeting, Seattle,WA, July 24-28 2005 *Med. Phys.* **32** 1900-1

Snyder D L, Miller M I, Thomas L I Jr and Politte D G 1987 Noise and edge artifacts in maximum-likelihood reconstructions for emission tomography *IEEE Trans. Med. Imaging* **MI-6** 228-38

Soret M, Bacharach S L and Buvat I 2007 Partial-volume effect in PET tumor imaging *J Nucl Med* **48** 932-45

Teo B K, Seo Y, Bacharach S L, Carrasquillo J A, Libutti S K, Shukla H, Hasegawa B H, Hawkins R A and Franc B L 2007 Partial-Volume Correction in PET: Validation of an Iterative Postreconstruction Method with Phantom and Patient Data *J Nucl Med* **48** 802-10

Tomic N, Thompson C J and Casey M E 2005 Investigation of the “Block Effect” on spatial resolution in PET detectors *IEEE Trans. Nucl. Sci.* **52** 599-605

Wallis J W and Miller T R 1993 Rapidly Converging Iterative Reconstruction Algorithms in Single-Photon Emission Computed Tomography *Journal of Nuclear Medicine* **34** 1793-800